Electronic Supplementary Material (ESI) for Environmental Science: Nano.
This journal is © The Royal Society of Chemistry 2024

# SUPPLEMENTARY FILE

## Waste-derived Carbon Nanodots for Fluorimetric and Simultaneous Electrochemical Detection of Heavy Metals in Water

Index



| **Sample** (time-Temperature) | **Hydrochar yields* (wt%) ± *sd*** |
|---|---|

| | |
|---|---|
| Hydrochar $_{(60–180)}$ | 15.35 ± 0.88 |
| Hydrochar $_{(60–210)}$ | 18.27 ± 1.11 |
| Hydrochar $_{(60–240)}$ | 24.27 ± 1.32 |
| Hydrochar $_{(90–180)}$ | 22.51 ± 0.95 |
| Hydrochar $_{(90–210)}$ | 31.09 ± 1.81 |
| Hydrochar $_{(90–240)}$ | 38.55 ± 1.02 |
| Hydrochar $_{(120–180)}$ | 18.05 ± 2.44 |
| Hydrochar $_{(120–210)}$ | 23.52 ± 1.53 |
| Hydrochar $_{(120–240)}$ | 27.10 ± 3.08 |

*hydrochar yield was calculated as follow (1): $$yield\ (wt\%) = \frac{g\ of\ product}{initial\ g\ of\ dry\ BB} \times 100$$

**Table S1.** BB-hydrochar yields

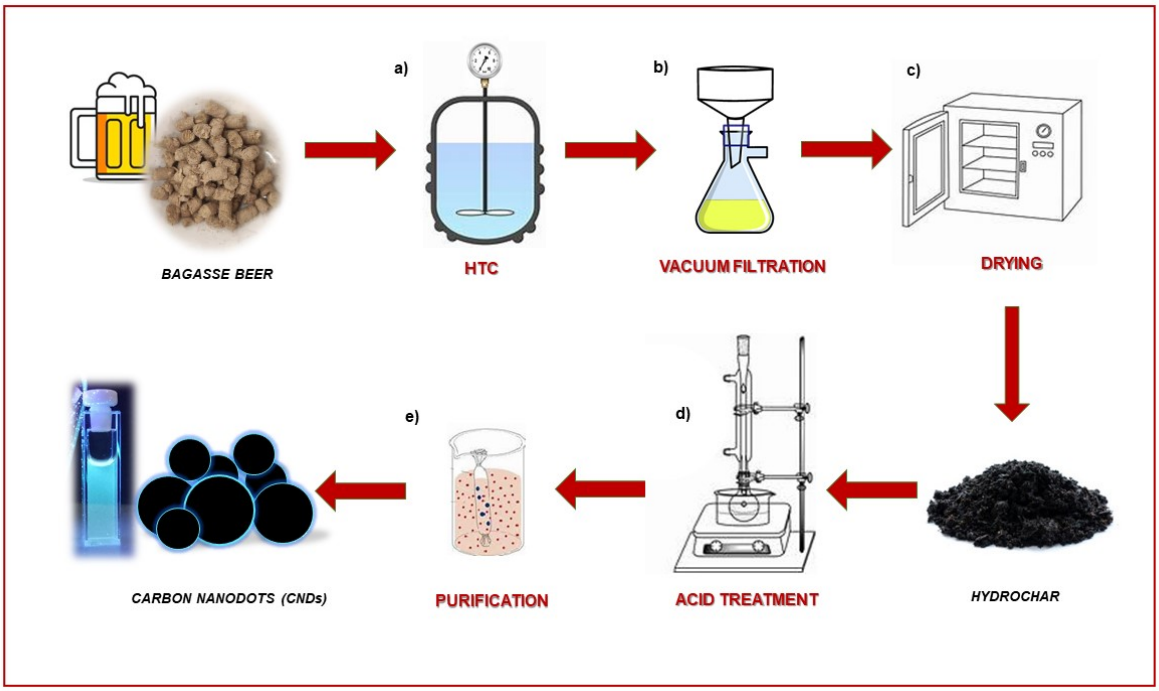


**Scheme S1.** Pathways involved in the preparation of CNDs from BB

The FTIR spectra of the feedstock and its hydrochar showed absorption peaks characteristic of lignocellulosic biomasses (Figure S1)(2). A strong broad band observed at 3300 $cm^{-1}$ is attributed to O–H stretching of cellulose hydroxyl groups. The weak absorption peaks between 2900-2850 $cm^{-1}$ were due to C–H stretching of the methylene groups (3). The peak at 1640 $cm^{-1}$ suggests the presence of amino groups, and the band between 1500 $cm^{-1}$ and 1160 $cm^{-1}$ correspond to the vibrations of C–

O–C and C–N (3). The strong peak observed at 1030 $cm^{-1}$ was attributed due to C–O stretching. The absorption peak detected at 550 $cm^{-1}$ was due to β-glycosidic bond between sugar monomers (2).

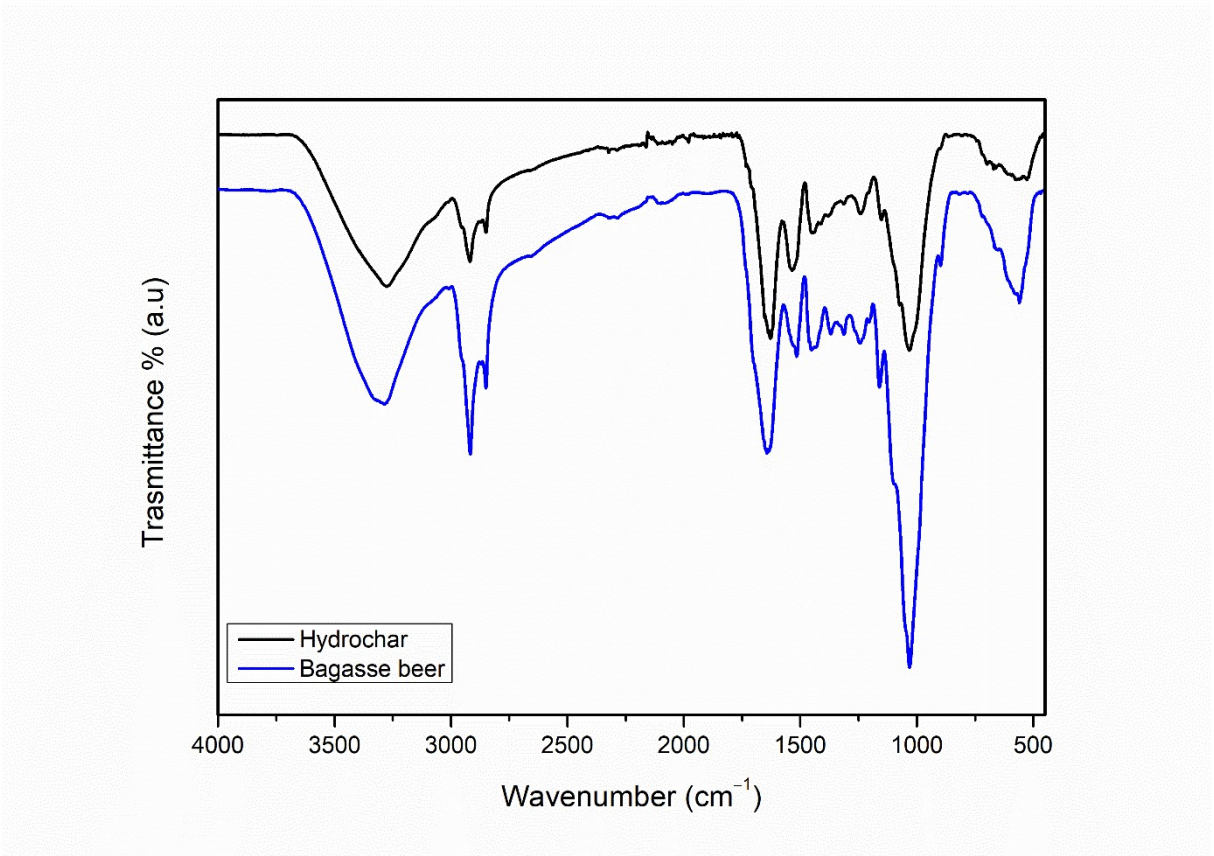


**Figure S1.** FTIR spectra of Bagasse beer (blue) and Hydrochar (black)

The DLS measurements were carried out in order to verify the size distribution profile and the presence of small particles in the raw materials. The DLS data (Figure S2) showed single size population centred 615 nm for the BB and two populations around 100 nm and 500 nm were observed for the hydrochar: these results suggest that the hydrothermal process helps to obtain nanomaterials but not smaller than 10 nm, therefore, subsequent treatments and purification processes were necessary to reduce the size and minimize the formation of these agglomerated clusters.

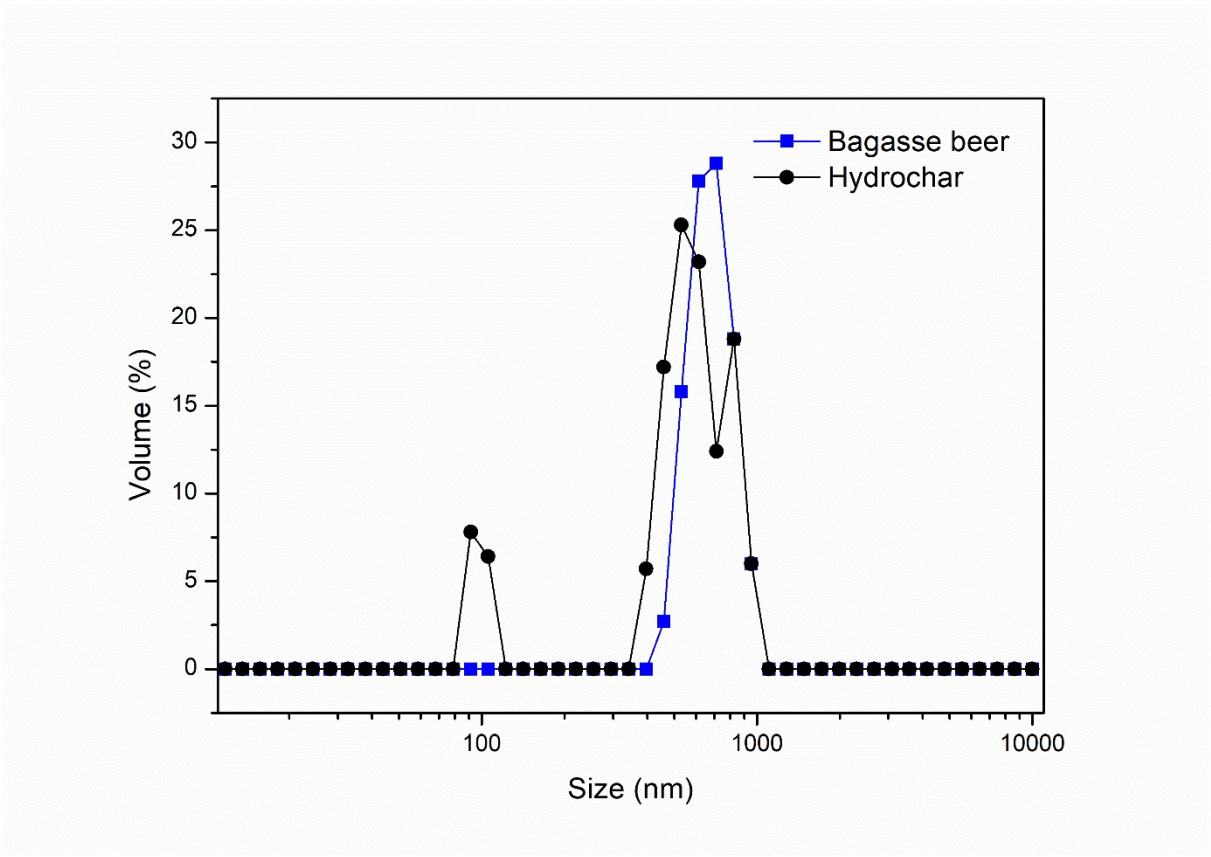


**Figure S2.** DLS distribution dimensions particles of bagasse beer (blue) and hydrochar (black)

The XRD spectra (Figure S3) show the crystalline cellulose peaks at 16 (101), 22.3 (002), and 35 (040) 2θ degrees, which are more pronounced in the starting material than in the hydrochar. This indicates that the hydrothermal treatment leads to a complete transformation of the "crystalline phase" to the "amorphous phase", considering the disappearance of the peak at 16 2θ (degree) (4). This phenomenon can also be attributed to the well-packed long chains of lignocellulose components in BB, which are characterized by strong hydrogen bonds(4). These hydrogen bonds facilitate the preservation of the sugar rings, which is further promoted by the depolymerisation and hydrolysis reactions occurring during the hydrothermal carbonization process(3).

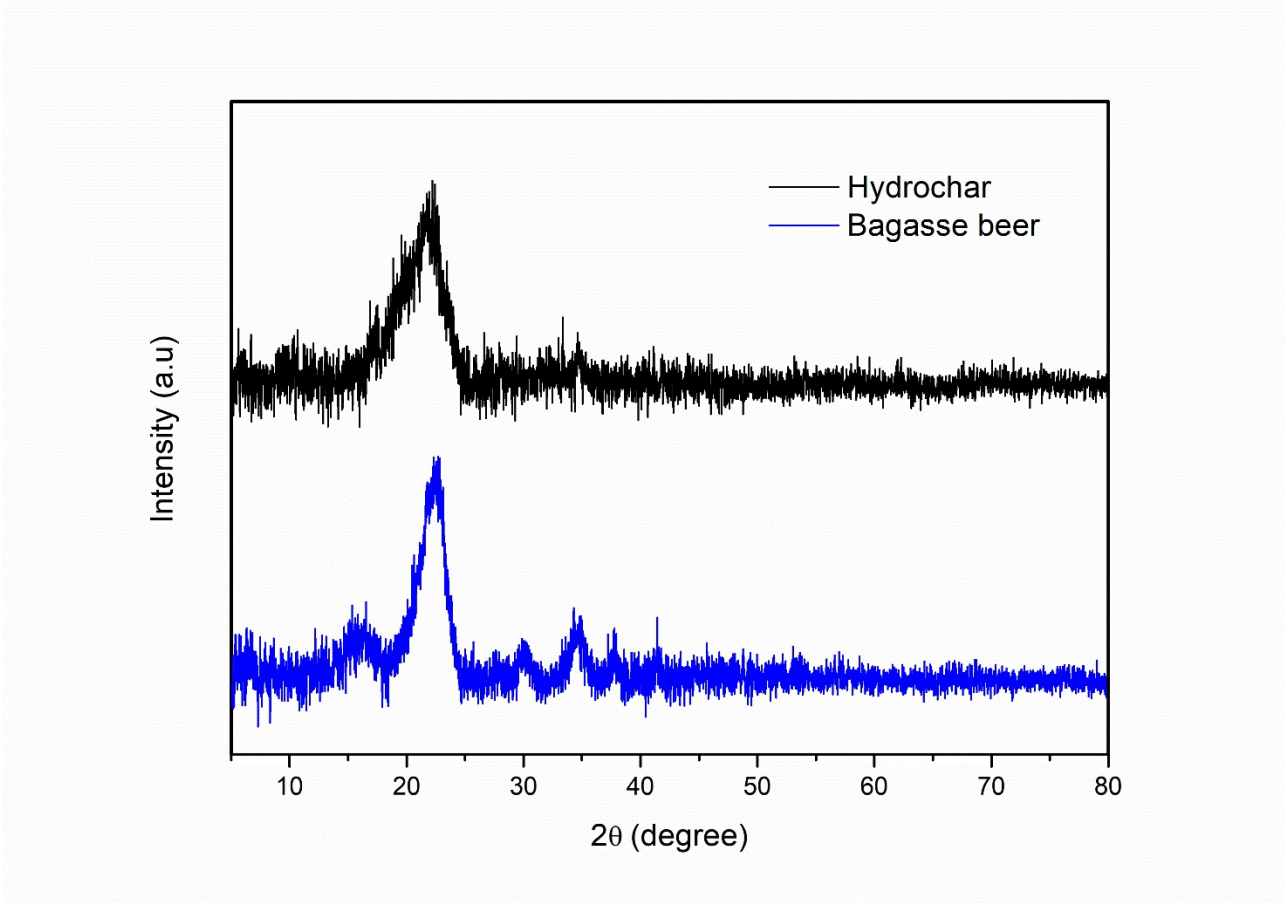


**Figure S3**. XRD spectra of bagasse beer (blue) and hydrochar (black) after baseline correction

| **Sample** | **C%** ± sd | **N%**± sd | **H%**± sd | **S%** | **O%**[a] |
|---|---|---|---|---|---|
| CNDs | 51.33 ± 1.05 | 6.84 ± 0.21 | 6.01 ± 0.25 | 0 | 35.82 |

[a]calculated by difference

**Table S2.** Results of CHNS elemental analysis of CNDs

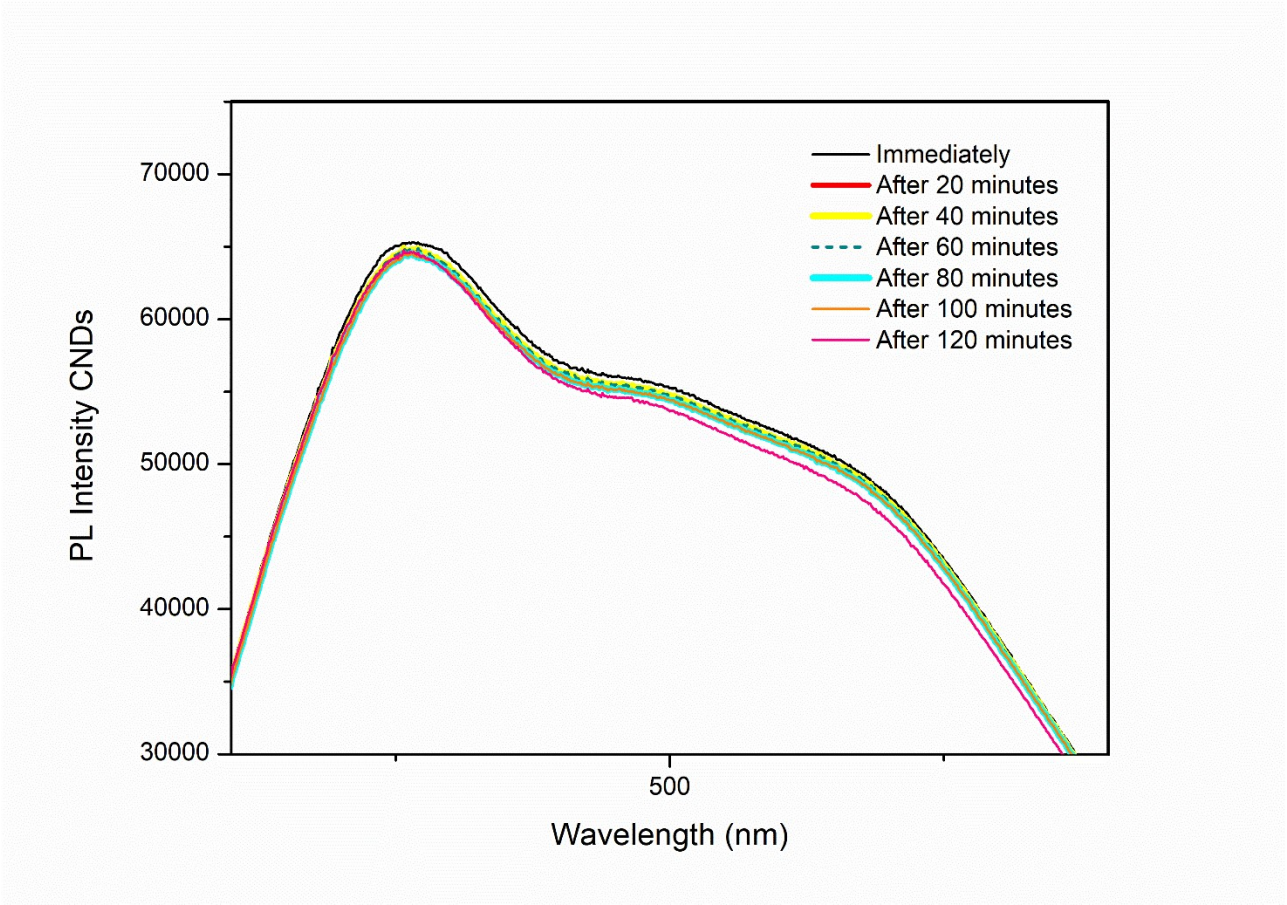


**Figure S4.** Photostability of CNDs

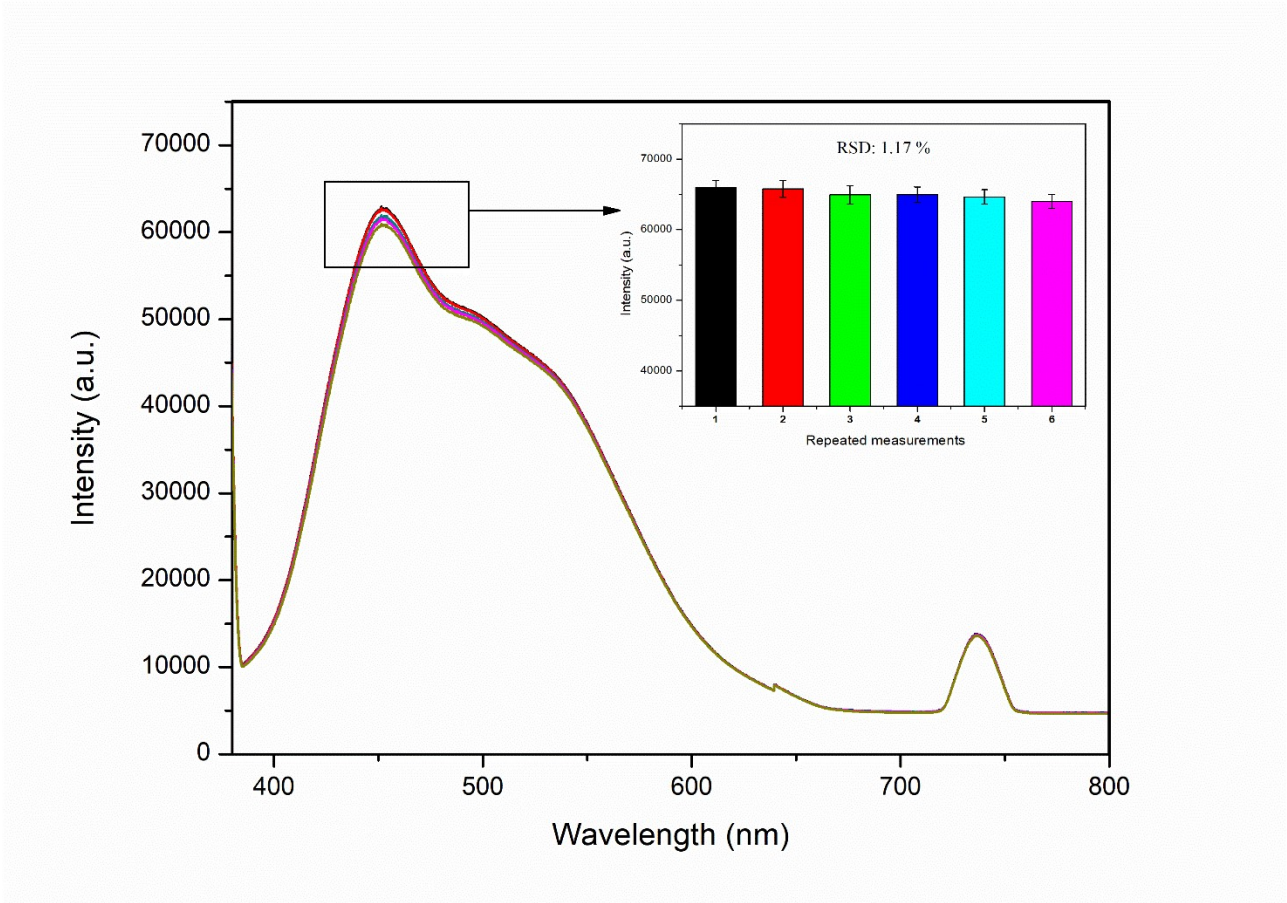


**Figure S5.** PL Measurement repeatability

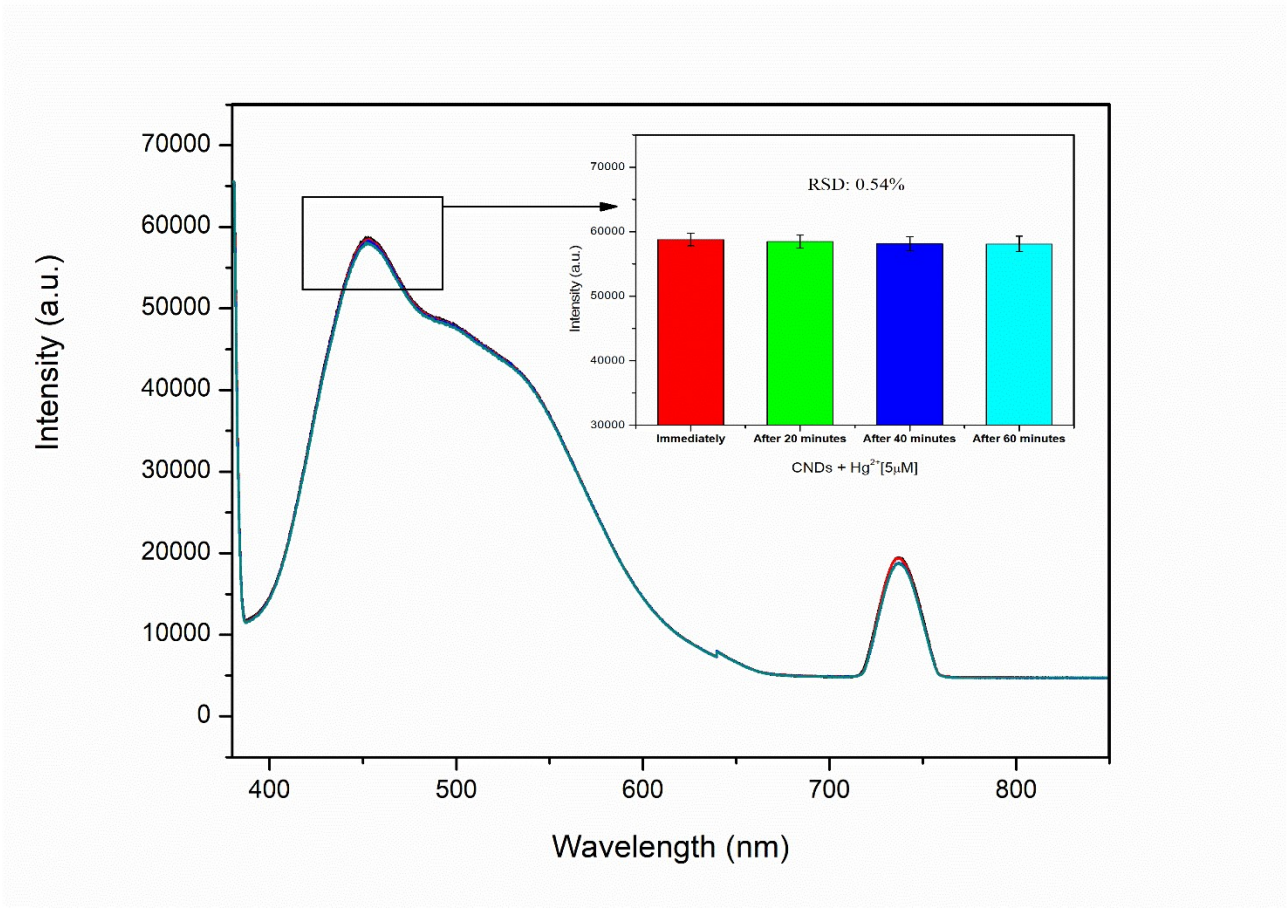


**Figure S6.** Stability PL response of CNDs with 5 μM of $Hg^{2+}$ monitored after 20 minutes, 40 minutes and 60 minutes

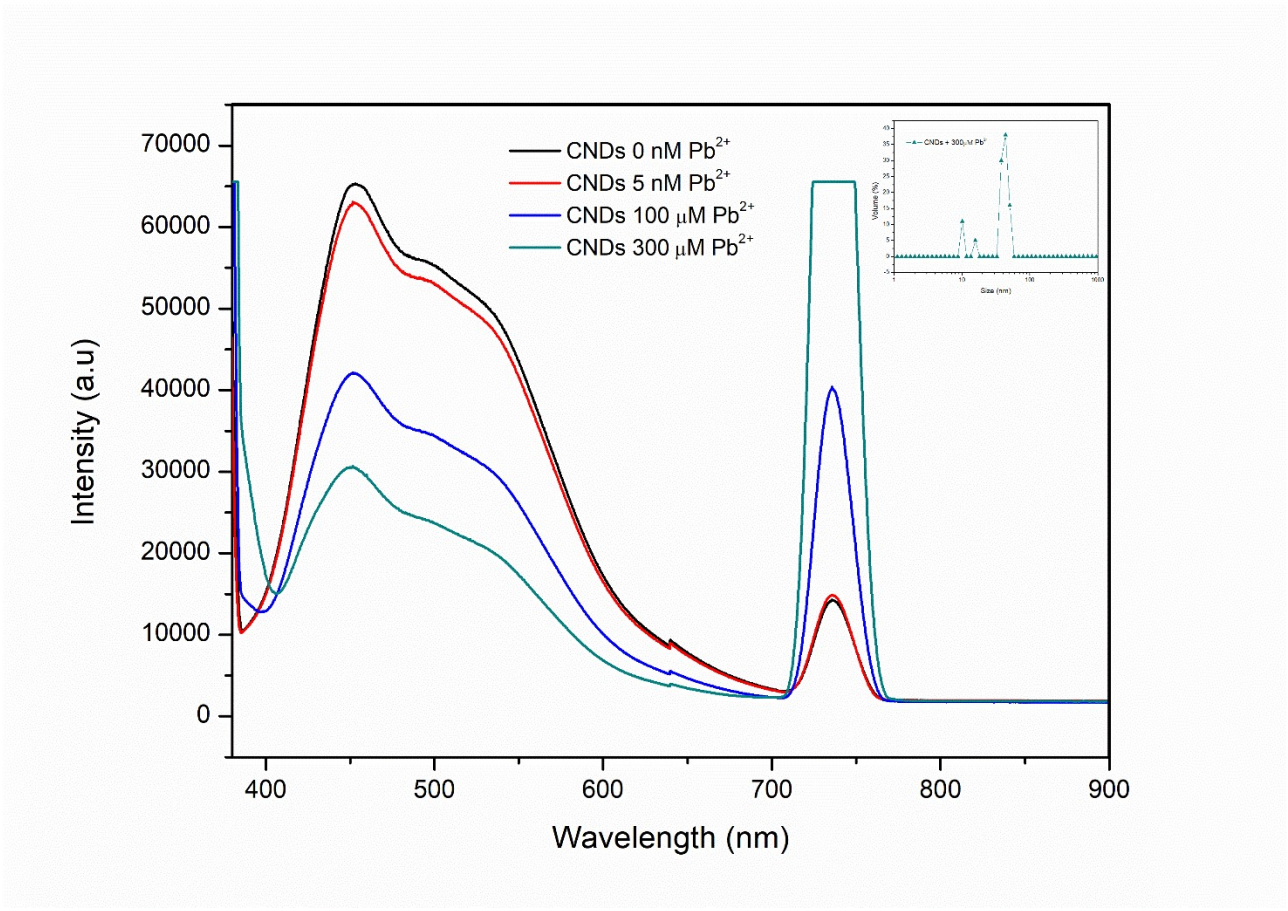


**Figure S7.** Second harmonic PL CNDs at different addition of $Pb^{2+}$ and (inset) related increasing of CNDs aggregation after 300 µM of $Pb^{2+}$ addition revealed by DLS measurement

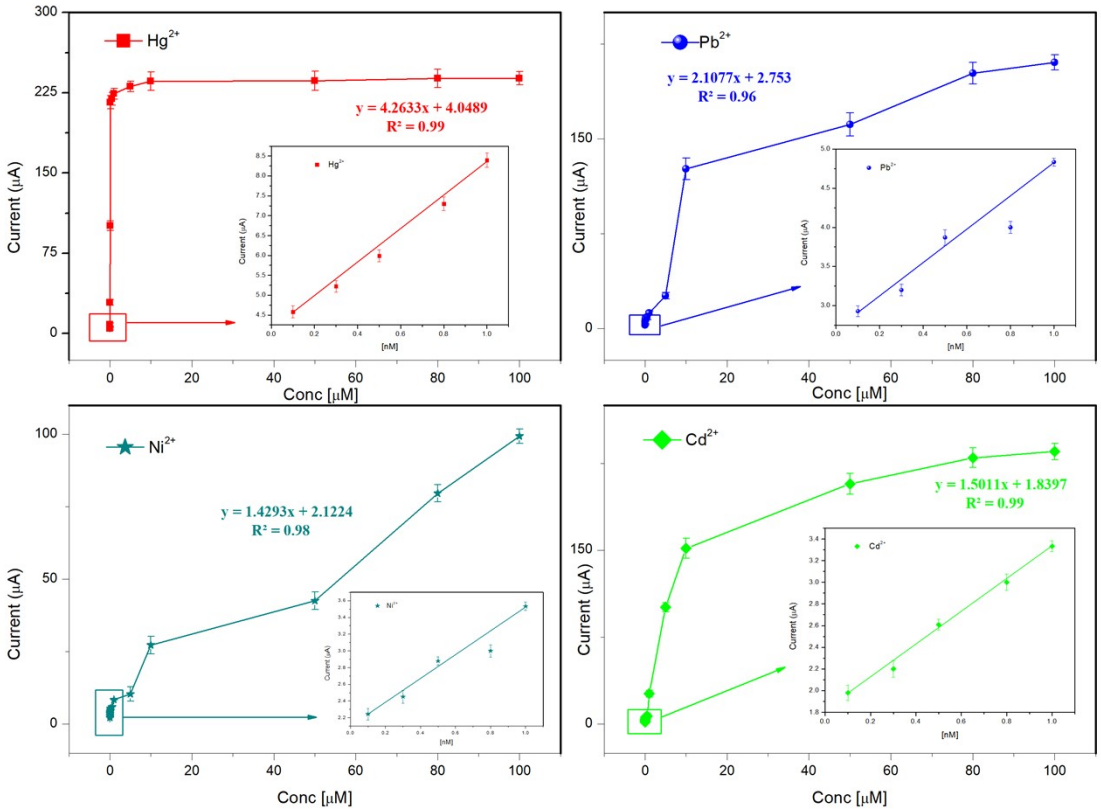


**Figure S8.** CNDs/SPCE response to $Hg^{2+}$, $Pb^{2+}$, $Ni^{2+}$ and $Cd^{2+}$ addition in the studied concentration range [0.1 nM to 100µM]; insets: calibration graphs for peak current at low concentrations [0.1 to 1 nM] and related fit linear equations (sd ≤ 3)

**Table S3.** Comparison of different fluorescent carbon nanodots derived from green sources for $Hg^{2+}$ and $Pb^{2+}$ photoluminescence (PL) detection

| Samples | Heavy metal ions detected | Detection techniques | LOD (µM) | Sensitivity ($\mu A n M^{-1} cm^{-2}$) | Ref. |
|---|---|---|---|---|---|
| CNDs-bagasse beer derived | $Hg^{2+}$ | PL | 0.011 | 883.44 | This work |
| | $Pb^{2+}$ | PL | 0.079 | 126.64 | This work |
| CNDs-fruit waste derived | $Hg^{2+}$ | PL | 55 | - | (5) |
| CNDs-fruit waste derived | $Hg^{2+}$ | PL | 0.33 | - | (6) |
| CNDs- Pigeon eggs or feathers derived | $Hg^{2+}$ | PL | 0.035 | - | (7) |
| | | PL | 0.039 | - | |
| | | PL | 0.010 | - | |

| | | | | | |
|---|---|---|---|---|---|
| CNDs-leaves derived | $Pb^{2+}$ | PL | 0.0006 | - | (8) |
| CNDs-citric acid derived | $Hg^{2+}$ | PL | 0.226 | - | (9) |
| CNDs-Microalgae derived | $Pb^{2+}$ | PL | 0.01 | - | (10) |
| CNDs-glutathione+formamide derived | $Hg^{2+}$ | PL | 0.039 | - | (11) |
| | $Pb^{2+}$ | PL | 0.037 | - | |
| CNDs-coconut milk derived | $Hg^{2+}$ | PL | 0.016 | - | (12) |

**Table S4.** Comparison of various carbon nanodots derived from green sources as electrochemical sensors for heavy metal ions detection

| Samples | Heavy metal ions detected | Detection techniques | LOD | Sensitivity ($\mu AnM^{-1}cm^{-2}$) | Ref. |
|---|---|---|---|---|---|
| CNDs-bagasse beer derived | $Hg^{2+}$ | SWV | 0.124 µg/L | 34.1 | This work |
| | $Pb^{2+}$ | SWV | 0.551 µg/L | 21.3 | This work |
| | $Cd^{2+}$ | SWV | 0.453 µg/L | 32.3 | This work |
| | $Ni^{2+}$ | SWV | 0.608 µg/L | 11.4 | This work |
| CNDs-activated carbon | $Pb^{2+}$ | SWASV[a] | 0.7 µg/L | 100.37 | (13) |
| | $Cd^{2+}$ | SWASV | 0.4 µg/L | 109.45 | |
| CNDs-leaves derived | $Pb^{2+}$ | DPASV[b] | 0.14 nM | - | (14) |
| GQDs[c] | $Pb^{2+}$ | SWASV | 8 µg/L | 100.37 | (15) |
| | $Cd^{2+}$ | SWASV | 11.30 µg/L | 109.45 | |
| CNDs-pomelo peels waste derived | $Pb^{2+}$ | SWASV | 12 nM | 0.11 | (16) |
| | $Cd^{2+}$ | SWASV | 13 nM | 0.11 | |

[a]SWASV: Square Wave Anodic Stripping Voltammetry; [b] DPASV: Differential Pulse Anodic Stripping Voltammetry; [c]GQDs: Graphene Quantum Dots.


1. Spagnuolo D, Iannazzo D, Len T, Balu AM, Morabito M, Genovese G, et al. Hydrochar from Sargassum muticum: a sustainable approach for high-capacity removal of Rhodamine B dye. RSC Sustain [Internet]. 2023 Jul 6 [cited 2023 Jul 19]; Available from: https://pubs.rsc.org/en/content/articlelanding/2023/su/d3su00134b

2. Pang SC, Voon LK, Chin SF. Controlled Depolymerization of Cellulose Fibres Isolated from Lignocellulosic Biomass Wastes. International Journal of Polymer Science. 2018 Jul 19;2018:1–11.

3. Saha N, McGaughy K, Reza MT. Elucidating hydrochar morphology and oxygen functionality change with hydrothermal treatment temperature ranging from subcritical to supercritical conditions. Journal of Analytical and Applied Pyrolysis. 2020 Nov 1;152:104965.

4. Satira A, Paone E, Bressi V, Iannazzo D, Marra F, Calabrò PS, et al. Hydrothermal Carbonization as Sustainable Process for the Complete Upgrading of Orange Peel Waste into Value-Added Chemicals and Bio-Carbon Materials. Applied Sciences. 2021 Jan;11(22):10983.

5. Durairaj A, Maruthapandi M, Luong JHT, Perelshtein I, Gedanken A. Enhanced UV Protection, Heavy Metal Detection, and Antibacterial Properties of Biomass-Derived Carbon Dots Coated on Protective Fabrics. ACS Appl Bio Mater. 2022 Dec 19;5(12):5790–9.

6. Desai ML, Jha S, Basu H, Singhal RK, Park TJ, Kailasa SK. Acid Oxidation of Muskmelon Fruit for the Fabrication of Carbon Dots with Specific Emission Colors for Recognition of Hg2+ Ions and Cell Imaging. ACS Omega. 2019 Nov 19;4(21):19332–40.

7. Ye Q, Yan F, Luo Y, Wang Y, Zhou X, Chen L. Formation of N, S-codoped fluorescent carbon dots from biomass and their application for the selective detection of mercury and iron ion. Spectrochimica Acta Part A: Molecular and Biomolecular Spectroscopy. 2017 Feb 15;173:854–62.

8. Kumar A, Chowdhuri AR, Laha D, Mahto TK, Karmakar P, Sahu SK. Green synthesis of carbon dots from Ocimum sanctum for effective fluorescent sensing of Pb2+ ions and live cell imaging. Sensors and Actuators B: Chemical. 2017 Apr 1;242:679–86.

9. Yan F, Zou Y, Wang M, Mu X, Yang N, Chen L. Highly photoluminescent carbon dots-based fluorescent chemosensors for sensitive and selective detection of mercury ions and application of imaging in living cells. Sensors and Actuators B: Chemical. 2014 Mar 1;192:488–95.

10. Plácido J, Bustamante-López S, Meissner KE, Kelly DE, Kelly SL. Microalgae biochar-derived carbon dots and their application in heavy metal sensing in aqueous systems. Science of The Total Environment. 2019 Mar 15;656:531–9.

11. Yarur F, Macairan JR, Naccache R. Ratiometric detection of heavy metal ions using fluorescent carbon dots. Environ Sci: Nano. 2019 Apr 11;6(4):1121–30.

12. Roshni V, Ottoor D. Synthesis of carbon nanoparticles using one step green approach and their application as mercuric ion sensor. Journal of Luminescence. 2015 May 1;161:117–22.

13. Lee J, Kim S, Shin H. Hierarchical Porous Carbon Electrodes with Sponge-Like Edge Structures for the Sensitive Electrochemical Detection of Heavy Metals. Sensors. 2021 Jan;21(4):1346.

14. Liu Q, Gao X, Liu Z, Gai L, Yue Y, Ma H. Sensitive and Selective Electrochemical Detection of Lead(II) Based on Waste-Biomass-Derived Carbon Quantum Dots@Zeolitic Imidazolate Framework-8. Materials. 2023 Jan;16(9):3378.

15. Pizarro J, Segura R, Tapia D, Navarro F, Fuenzalida F, Jesús Aguirre M. Inexpensive and green electrochemical sensor for the determination of Cd(II) and Pb(II) by square wave anodic stripping voltammetry in bivalve mollusks. Food Chemistry. 2020 Aug 15;321:126682.

16. Zhang T, Jin H, Fang Y, Guan J, Ma S, Pan Y, et al. Detection of trace Cd2+, Pb2+ and Cu2+ ions via porous activated carbon supported palladium nanoparticles modified electrodes using SWASV. Materials Chemistry and Physics. 2019 Mar 1;225:433–42.